

# Oscillation in a Network Model of Neocortex

Jennifer Dwyer<sup>1</sup>, Hyong Lee<sup>1</sup>, Amber Martell<sup>1</sup>,  
Rick Stevens<sup>2,3</sup>, Mark Hereld<sup>2,3</sup>, and Wim van Drongelen<sup>1,2</sup>

<sup>1</sup> The University of Chicago, Department of Pediatrics, 5841 South Maryland Avenue,  
Chicago, IL, 60637, USA

<sup>2</sup> The University of Chicago, Computation Institute, 5640 South Ellis Avenue,  
Chicago, IL, 60637, USA

<sup>3</sup> Argonne National Laboratory, Mathematics and Computer Science Division, 9700  
Cass Avenue, Argonne, IL, 60439, USA

## 1 Introduction

Brain activity can be studied at multiple levels, ranging from synapses to single neurons to networks of millions of nerve cells. Gaining understanding of the complex, opaque relationships between activities across the microscopic and macroscopic levels is a major goal in neuroscience, because it would be a tremendous help to unravel the underpinning of both normal and pathological function. For example, one would be able to describe how individual neural components interact to generate the  $\gamma$ -rhythm of the electroencephalogram (EEG), how neurons go awry during an epileptic seizure, or how they generate a steering signal for a muscle group.

Current experimental techniques cannot capture the behavior of all the individual neural components of a large network in sufficient detail: electrophysiology lacks the spatial resolution for measuring individual cells in a network, while imaging techniques lack temporal resolution. Data collected from computational models of neural networks are not thus limited and therefore can reveal individual and aggregate neuronal activity at the same time [12, 17, 18, 19, 20].

Traditional network models usually contain neurons with integrate-and-fire properties. Recently it was recognized that neurons can also have inductor-like resonant characteristics (reviewed in [8]). Depending on the voltage-dependence of stabilizing ion channels, these characteristics can be simulated with models that include biophysically realistic channels (e.g., [9]). Since brain rhythms are believed to play a critical role in neural processing (e.g., [3]), it is important to establish how such resonant properties affect network dynamics.

The purpose of this study is to model and examine the relationship between cellular and network oscillations. We examine network activity in a previously developed neuronal model of neocortex with biophysically realistic ion channels following the Hodgkin and Huxley formalism [7, 11, 19, 20]. We determine the resonant properties of single neocortical cells and study how these properties relate to onset and offset of network oscillations.

## 2 Methods

### *Modeling.*

Because the histo-physiology of neocortex is not described at the same level of detail as other areas in the brain, such as hippocampus, we focus on replicating the general network characteristics of neocortical circuitry. Therefore we include excitatory and inhibitory neuronal populations, recurrent excitation, inhibition, disinhibition, direct electrical contact between the inhibitory cell types, and feedback and feedforward loops. Because thalamic input is not of primary interest for intrinsic cortical oscillations, we focus on the pyramidal neurons and neglect stellate cells. Inhibitory neurons, although a minority in the cortex, are more variable than the excitatory neuronal population. In the current model we focus on the inhibitory neurons that predominantly connect to soma and initial segment and that have significant horizontal spread (relevant for propagation of cortical activity).

Details of the model are described in [18, 19, 20]. Briefly, the neural network representing neocortex includes excitatory and inhibitory neuronal populations with a multicompartamental representation for each cell type. Sodium and potassium channels following the Hodgkin and Huxley formalism are included in the soma and initial segment compartments of the cell models. Excitatory synaptic function was simulated with an alpha function (time constant 1-3 ms), while inhibitory synaptic activity was modeled by a dual exponential function with time constants of 1 and 7 ms.

The excitatory component of the network (Fig. 1) consists of superficial pyramidal cells from cortical layers 2/3 (S, Fig. 1) and deep pyramidal cells from layers 5/6 (D, Fig. 1). The network inhibition is provided by three types of basket cells and the chandelier cell (I, Fig. 1), all of which receive input from both types of pyramidal neurons. The basket cells inhibit the pyramidal cell soma, whereas the chandelier cells directly inhibit the initial segment. The model captures essential features of neocortical microcircuitry: we use a ratio of 4:1 for excitatory to inhibitory neurons; excitatory synapses end on the dendritic portion and the inhibitory ones on the soma, initial segment, and dendrites [4]; connections include recurrent excitation, reciprocal inhibitory contacts, axo-axonic interneurons, and nearest-neighbor gap junctions (R, Fig. 1) between inhibitory cells [1]. The neurons are placed in a three-dimensional grid with realistic cell density and network connectivity based on histological and physiological studies [4, 5, 6, 10, 13, 14].

The computational model is implemented in the parallel GENESIS neural simulator [2]. Extracellular activity was obtained as the weighted sum of currents generated by the model cells' somas [15]. Depending on the overall levels of synaptic excitation  $E$  and inhibition  $I$ , the model displays a variety of EEG rhythms; for example, with  $I=2.0$ , the model produces desynchronized activity ( $E \sim 3.0$ ), network bursts ( $E < 0.5$ ), or oscillations around 28 Hz ( $0.5 < E < 3.0$ ) [18].

Two sets of simulations were performed. In the first, one of each cell type in a 656-cell network was primed with a 300 pA current injection for 200 ms; thereafter, the simulation was allowed to progress without further stimulation. The network coupling ( $E$  &  $I$ ) were set so that the network would oscillate. In the second set of simulations, the response of the model neurons and network to the frequency of external stimulation was evaluated by injecting sinusoidal currents. A 1 nA current (1-100 Hz) applied to the soma of a single model cell elicited a response just below its spiking threshold. Network stimulation during bursting activity was modeled by injecting a 30 pA sinusoidal current into 25% of the superficial pyramidal cells in their distal apical dendrite compartments. We varied the frequency of this current between 1 and 300 Hz.

**Experimental Procedures.** Coronal slices (500  $\mu\text{m}$ ) were prepared from CD-1 mice ages P8-12 and transferred into artificial cerebral spinal fluid (ACSF) consisting of (in mM) 118 NaCl, 25 NaHCO<sub>2</sub>, 30 glucose, 3 KCl, 1 NaH<sub>2</sub>PO<sub>4</sub>, 1 CaCl<sub>2</sub>, and 1 MgCl<sub>2</sub> (pH 7.4). Patch pipettes and electrodes for extracellular recordings were manufactured from glass capillaries and filled with intracellular solution containing (in mM) 140 D-gluconic acid, 10 EGTA, 10 HEPES, 2 MgCl<sub>2</sub>, 1 CaCl<sub>2</sub>, 4 Na<sub>2</sub>ATP (pH 7.2). Layer 5 pyramidal neurons in the frontal cortex were patched using the blind-patching technique. The resonant properties of each neuron were measured by recording the cellular voltage response to intracellularly-injected sinusoidal current stimuli that ramped linearly in frequency from 0 to 15 Hz over 30 seconds (ZAP input). Extracellular recordings were performed in layer 5/6 frontal cortex using pipettes filled with bath ACSF solution. Network resonance was evaluated by delivering the ZAP current through a second stimulation electrode placed in layer 5/6. The measurement was repeated after blocking action potential generation (and synaptic transmission) by bath application of 1 mM tetrodotoxin (TTX) in order to verify the biological origin of the signal.

### 3 Results

***Role of Neuronal Resonant Properties in Network Oscillation.*** A sample of the EEG generated by the simulated neocortical patch is shown in Fig. 2A and the corresponding amplitude spectrum in Fig. 2B. These oscillations are also observed in the membrane potentials of individual neurons in the simulation (Fig. 2C, D). Although different cells show very different suprathreshold (spiking) behavior during the network oscillation, their subthreshold oscillations are remarkably similar and synchronized (Fig. 2C). Frequency analysis of each neuron's activity shows a strong component around 28 Hz, the same frequency as the EEG oscillation. The dominant peak in the amplitude spectrum reflects the predominant frequency of the subthreshold oscillations; while, the harmonics correspond to the varying degrees of spiking behavior among individual neurons. When isolated model neurons are stimulated with sinusoidal signals of varying frequencies, their responses display a resonant peak around 30 Hz (Fig. 2E, F): not identical, but very close, to the dominant frequency of the network oscillations.

***Offset of Network Bursting in the Model.*** In a second set of simulations we evaluated how effectively one might stop network bursting patterns with electrical stimulation. The upper trace in Fig. 5A depicts the EEG of a bursting network, and the six bottom traces show examples of how the EEG is altered by electrical stimulation with a sinusoidal current of different frequencies (ranging between 2 and 127 Hz). The graph in Fig. 5B shows how well different frequencies attenuate the network bursts. The stimulus is most effective in the range of the cellular resonance (~30 Hz).

***The Membrane Equivalent Circuit and Resonance.*** The close relationship observed between the resonant behavior of individual neurons and the dominant oscillatory frequency of the network has important implications for elucidating mechanisms underlying oscillatory behavior across macroscopic and microscopic levels. To analyze how intra-cellular components might contribute to resonance, we follow [8] and represent the electrical properties of a neuronal membrane as a parallel RLC circuit (see Fig. 3A,B). The fundamental concept is that passive properties of the cell membrane (i.e., membrane resistance  $R$  and membrane capacitance  $C$ ) interact with

an active current or currents (represented by the inductor in series with a resistor). As a whole, the circuit acts as a band-pass filter: in other words, it exhibits resonance.

From a dynamical systems point of view, the RC portion of the circuit can be described by a one-dimensional system whose equilibrium at rest is a node and is therefore incapable of producing oscillatory behavior. A simple parallel RC circuit can be used to model the linear subthreshold behavior of an integrator-type neuronal membrane. In order to model the properties of resonator neurons, a second dimension must be incorporated so that oscillations are possible near rest. A so-called resonate-and-fire (RF) neuron is the simplest example of a linear, two-dimensional model system that exhibits resonator-like properties [9, 16]. Furthermore, the RF neuron's subthreshold behavior can be modeled by the equivalent circuit shown in Fig. 3B, a simplified version of the Hodgkin and Huxley neuronal membrane model [7] depicted in Fig. 3A. The inductor-resistor series component of the circuit in Fig. 3B is a good model for an ion channel capable of producing resonance. An inductor, which generates an electromotive force that opposes the injected current to the circuit, is analogous to a resonant channel, such as the delayed rectifier potassium channel, that can oppose changes in membrane voltage by, for example, activating outward current upon depolarization.

To gain a more intuitive understanding of how resonance arises in the cell, we approximate the RLC impedance curve as follows. First, we consider the effective impedance ( $Z_{RC}$ ) for the resistor ( $R_m$ ) and capacitor ( $C_m$ ) in parallel separately from the impedance for the inductor ( $L_K$ ) and resistor ( $R_K$ ) in series ( $Z_{LR}$ ). From the usual rule for adding impedances in parallel,  $\frac{1}{Z_{RC}} = \frac{1}{Z_{R_m}} + \frac{1}{Z_{C_m}} = \frac{1}{R_m} - \frac{i}{2\pi f C_m}$ . As a result,  $|Z_{RC}|$  must be smaller than either  $|Z_{R_m}|$  or  $|Z_{C_m}|$  (these limits, with the exact solution for  $|Z_{RC}|$ , are shown and labeled accordingly in Fig. 3C). We also note that  $Z_{LR} = Z_{L_K} + Z_{R_K} = i2\pi f L_K + R_K$ , so that  $|Z_{LR}|$  must be greater than either  $|Z_{L_K}|$  or  $|Z_{R_K}|$  (dotted line, indicated  $L_K R_K$ , in Fig. 3C). Finally, the effective impedance for the entire circuit,  $Z$ , is given by  $\frac{1}{Z} = \frac{1}{Z_{LR}} + \frac{1}{Z_{RC}}$ ; neglecting for the moment the relative phase angle of the components,  $|Z|$  can be approximated as being less than either  $|Z_{RC}|$  or  $|Z_{LR}|$ . As the exact solution to  $|Z|$  (dotted curve indicated "whole cell impedance" in

Fig. 3C) illustrates, combining these constraints can help estimate whether, and at what frequency, a resonant peak exists in the cell's impedance curve. Conversely, it is possible to estimate the values of the circuit elements from the impedance curve.

**Properties of Ion Channels and Resonance.** Simplifying further, if the circuit in Fig. 3B is under voltage clamp, we can disregard the contribution of the  $C_m$  branch (because the membrane is charged directly by the voltage clamp electrode, not through the membrane resistance, the voltage across the capacitor tracks the set point voltage rapidly compared to any timescales relevant to the channels in the membrane). If, in addition, we consider just the conductance due to potassium (e.g., if all other channel types are blocked pharmacologically), the circuit reduces to only the  $R_K$  and  $L_K$  components in series with the voltage clamp command potential  $V$  (Fig. 3D). This simplified circuit allows us to describe the current response (the output measured in a voltage clamp experiment) to a voltage step as follows:

$$I(t) = \frac{V}{R_K} \left( 1 - e^{-\frac{R_K t}{L_K}} \right).$$

The channel time constant  $\tau_K$  is equal to  $\frac{L_K}{R_K}$ , so finding the values of  $L_K$  and

$R_K$  provides the time constant of the ion channel (or channels) primarily responsible for the resonance peak (see the impedance plots in Fig. 3C:  $L_K$  is estimated from the value of the total impedance at the resonance peak, while  $R_K$  is roughly the low-frequency baseline value of the total impedance).

We now show an example of how to calculate  $\tau_K$ . Fig. 2F shows the impedance curve from a model pyramidal cell; point 3 indicates the impedance  $Z_{res}$  at the resonant frequency  $f_{res}$ , point 1 shows the low frequency limit of the impedance  $Z_1$  at  $f_1 \ll f_{res}$  and point 2 indicates the impedance  $Z_2$  at a high frequency  $f_2 \gg f_{res}$ . To estimate the channel time constant:

- (1) Find  $C_m$  from  $f_2, Z_2$ : At  $f_2$  the capacitor contributes most of the impedance  $Z_2$  (see Fig. 3C), so  $C_m$  can be estimated by substituting  $f_2 = 61.35$  Hz and

$$|Z_2| = 50 \text{ M}\Omega \text{ into } C_m = \frac{1}{(2\pi f_2 |Z_2|)} = 5.2 \times 10^{-5} \text{ }\mu\text{F}.$$

- (2) Estimate  $L_K$  from  $f_{res}, C_m$ : At  $f_{res}$ , the total impedance consists of roughly equal contributions from the capacitor and inductor:

$$|Z_{C_m}| \approx |Z_{L_k}| \rightarrow \frac{1}{2\pi f_{res} C_m} \approx 2\pi f_{res} L_K \rightarrow L_K = \frac{1}{4\pi^2 f_{res}^2 C_m} \text{ (in Henrys).}$$

Substituting  $C_m$  from (1) and  $f_{res} \approx 30$  Hz (see Fig. 2F) gives  $L_K \approx 0.54$  MH.

- (3) Find  $R_K$  from  $Z_I$ : Suppose we determine the value of  $R_m$  to be 170 M $\Omega$  by delivering a hyperpolarizing current step. From Fig. 2F, the impedance  $|Z_I| \approx 50$  M $\Omega$ ; since the current is quasi-static at  $f_I$ , we consider only the resistors and estimate  $R_K$  from  $\frac{1}{R_K} = \frac{1}{|Z_I|} - \frac{1}{R_m} \rightarrow R_K = 70$  M $\Omega$ .

- (4) We can now estimate the time constant  $\tau_K = \frac{L_K}{R_K} \approx 7.7$  ms.

That these estimates land fairly close to the actual model parameters ( $R_K = 68$  M $\Omega$ ;  $C_m = 5.8 \times 10^{-5}$   $\mu$ F;  $L_K = 0.38$  MH;  $\tau_K = 5.7$  ms) indicates that potassium channels play the principal role in shaping resonance in the model.

We tested for the presence of resonance in mouse *in vitro* neocortical networks by injecting current according to the ZAP protocol both to individual cells and via an extracellular electrode to stimulate the network (Fig. 4). Although an order of magnitude below the resonant peak in our model ( $\sim 2$  Hz versus  $\sim 30$  Hz in the model), we did observe similar principles at work: the frequency of the cellular and network resonances are nearly equal (the ratio between cellular and network resonance frequency in both the model and real neurons is  $\sim 1$ ). Blocking communication (with TTX) resulted in loss of resonance in the network. The purpose of adding TTX was to show that the network resonance was a biological signal rather than artifact; block of the frequency-dependent network effect by TTX could be due either to individual cells or loss of emergent network properties. Using the same procedure as described for the model pyramidal cell above, we calculated the time constant of the channel(s) responsible for shaping resonance observed experimentally in the real neurons (e.g., Fig. 4A) to be  $\sim 300$  ms.

## 4 Discussion

Although one would expect the suprathreshold behavior of neurons to be most important for the network's activity, and therefore the generated local field potentials and EEG, we show that subthreshold resonant behavior may determine spike timing and that synchronized subthreshold oscillation significantly contributes to the compound electrical activity generated by the population of neurons in the network. We acknowledge that it is difficult to unravel cause and effect, and that mechanisms promoting oscillations as an emergent property of the network's spiking activity offer possible explanations; however, the population of cells in the network creates sufficient activity to sustain oscillations in the neuron's membrane potential and the likelihood of sustained oscillations is highest near the peak of the single-cell resonance curve. These subthreshold oscillations affect the probability of action potential generation (Fig. 2C), thereby influencing overall spike timing in the network. At reasonable levels of spiking activity, the subthreshold oscillations in individual neurons become synchronized and together generate an oscillating extracellular current observable in the EEG signal. From the perspective of the network function, the oscillatory activity propagates back and forth between the superficial and deep layers [20].

From the analysis of the cell model's membrane equivalent circuit (Fig. 3), we confirm that the resonate-and-fire behavior seen in Fig. 2C can be explained with the inductive properties of the membrane [8]. To the best of our knowledge this is the first procedure that directly relates induction to the time constant of the membrane's resonant ion currents. We validate this procedure in our model by correctly estimating the known time constant of the  $K^+$  channel from the impedance measurement of the pyramidal cell in Fig. 2F. Applying this relationship between the cell's impedance and the resonant current to data recorded from slices of mouse neocortex, we show that inductive properties in real neurons are associated with a time constant of several hundred milliseconds. This estimate indicates that the ion current responsible is significantly slower than the delayed rectifier potassium current. Thus if, as in our model neurons, potassium channels play a major role in the resonance we observed in mouse neocortical pyramidal neurons, we can exclude channels with relatively rapid activation (such as  $K_{DR}$  or  $K_A$ ) from consideration; more probable contenders such as  $K_M$  must be further investigated experimentally.

The ultimate goal of our computational modeling effort is to create a virtual nervous system. In such a virtual environment one can study spontaneous and

perturbed activity patterns, thereby generating insight into neural function across scales. In our example, presented in Fig. 5, we show a relationship between the effectiveness of electrical stimulation of the network and the resonant frequency of the neurons. Insight into relationships across scales not only sheds light on brain function and malfunction, but it can also be used for computer-aided design of brain-computer interfaces. This approach may help to determine what signals are most effective as steering input to an interface (e.g., for a robotic arm), or it may provide a strategy for developing algorithms to decompose compound signals into more effective individual steering components.

## **Acknowledgements**

This work was supported by the Falk Foundation; the National Science Foundation (CNS-0509332); the Office of Advanced Scientific Computing Research, Office of Science, U.S. Dept. of Energy under Contract DE-AC02-06CH11357; the American Epilepsy Society; the ARCS Foundation; and the University of Chicago MSTP and GDTP training programs.

## **References**

- [1] Y. Amitai, J.R. Gibson, M. Beierlein, S.L. Patrick, A.M. Ho, B.W. Connors, and D. Golomb, The spatial dimensions of electrically coupled networks of interneurons in the neocortex, *J Neurosci.* 22 (2002) 4142-4152.
- [2] J.M. Bower and D. Beeman, *The Book of Genesis* (Springer Verlag, New York, 1998).
- [3] G. Buzsáki, *Rhythms of the brain* (Oxford University Press, New York, 2006).
- [4] J. DeFelipe, L. Alonso-Nanclares, and J.I. Arellano, Microstructure of the neocortex: comparative aspects, *J. Neurocytol.* 31 (2002) 299-316.
- [5] D. Feldmeyer and B. Sakmann, Synaptic efficacy and reliability of excitatory connections between principle neurones of the input (layer 4) and output (layer 5) of the neocortex, *J. Physiol.* 525 (2000) 31-39.
- [6] B.A. Hellwig, A quantitative analysis of the local connectivity between pyramidal neurons in layer 2/3 of the rat visual cortex, *Biol Cybern.* 82 (2000) 111-121.
- [7] A.L. Hodgkin and A.F. Huxley, A quantitative description of membrane current and its application to conduction and excitation in nerve, *J. Physiol.* 117 (1952) 500-544.
- [8] B. Hutcheon and Y. Yarom, Resonance, oscillation and the intrinsic frequency preferences of neurons, *Trends Neurosci.* 23 (2000) 216-22.
- [9] E.M. Izhikevich, *Dynamical Systems in Neuroscience: The Geometry of Excitability and Bursting* (MIT Press, Cambridge, MA, 2007).
- [10] L.S. Krimer and P.S. Goldman-Racik, Prefrontal microcircuits: Membrane properties and excitatory input of local, medium and wide arbor interneurons, *J. Neurosci.* 21 (2001) 3788-3796.

- [11] H.C. Lee, M. Hereld, R. Stevens, and W. Van Drongelen, Epileptiform activity patterns in coupled neural networks, 5th International Conference BEM & NFSI, Minneapolis, MN, 2005.
- [12] W.W. Lytton, Computer modelling of epilepsy, *Nat. Rev. Neurosci.* 9 (2008) 626-637.
- [13] V.B. Mountcastle, The columnar organization of the neocortex, *Brain* 120 (1997) 701-722.
- [14] R. Nieuwenhuys, The neocortex: An overview of its evolutionary development, structural organization and synaptology, *Anat. Embryol.* 190 (1994) 307-337.
- [15] P.L. Nunez, *Electric fields of the brain: the neurophysics of EEG* (Oxford University Press, Oxford, 1981).
- [16] S.H. Strogatz, *Nonlinear Dynamics and Chaos: With Applications to Physics, Biology, Chemistry, and Engineering* (Da Capo Press, Cambridge, MA, 2001).
- [17] R.D. Traub, D. Contreras, M.O. Cunningham, H. Murray, F.E. LeBeau, A. Roopun, A. Bibbig, W.B. Wilent, M.J. Higley, and M.A. Whittington, Single-column thalamocortical network model exhibiting gamma oscillations, sleep spindles, and epileptogenic bursts, *J. Neurophysiol.* 93 (2005) 2194-2232.
- [18] W. van Drongelen, H.C. Lee, H. Koch, M. Hereld, F. Elsen, Z. Chen, and R.L. Stevens, Emergent epileptiform activity in neural networks with weak excitatory synapses, *IEEE Trans. Neur. Sys. & Rehab.* 13 (2005) 236-241.
- [19] W. van Drongelen, H. Koch, F.P. Elsen, H.C. Lee, A. Mrejeru, E. Doren, C.J. Marcuccilli, M. Hereld, R.L. Stevens, and J.M. Ramirez, The role of persistent sodium current in bursting activity of mouse neocortical networks in vitro. *J. Neurophysiol.* 96 (2006) 2564-2577.
- [20] W. van Drongelen, H.C. Lee, R.L. Stevens and M. Hereld, Propagation of seizure-like activity in a model of neocortex, *J. Clin. Neurophysiol.* 24 (2007) 182-188.

## Figures

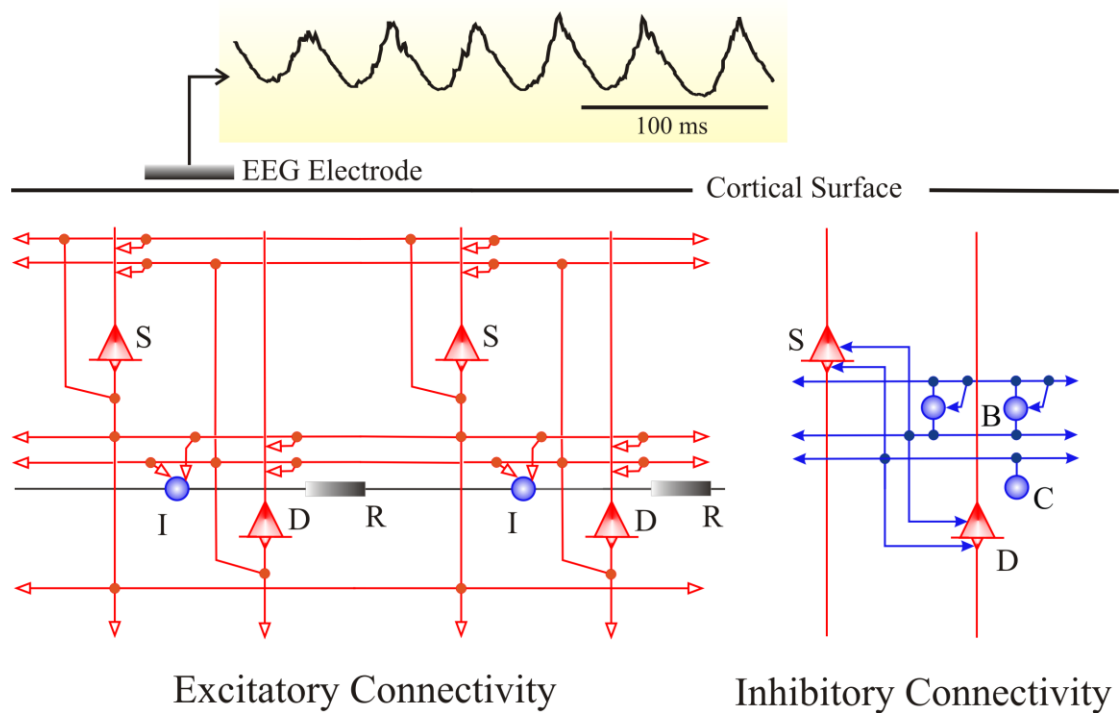


**Fig. 1:** Diagram of the neocortical model and the associated EEG electrodes. Included are superficial pyramidal neurons (S), deep pyramidal cells (D), and inhibitors (I). The pyramidal cells are the excitatory component with short-range and long-range connections (in steps of ~1 mm), the inhibitors inhibit the pyramidal cells and each other and have only short-range connections (not shown in the diagram). Each type of inhibitory neuron has interconnections via gap junctions, indicated by the resistor symbol (R). During oscillatory activity, symbolized with the stippled arrows, there is activity propagating between the superficial and deep layers. These oscillations are reflected in the compound signals recorded from the EEG electrodes.

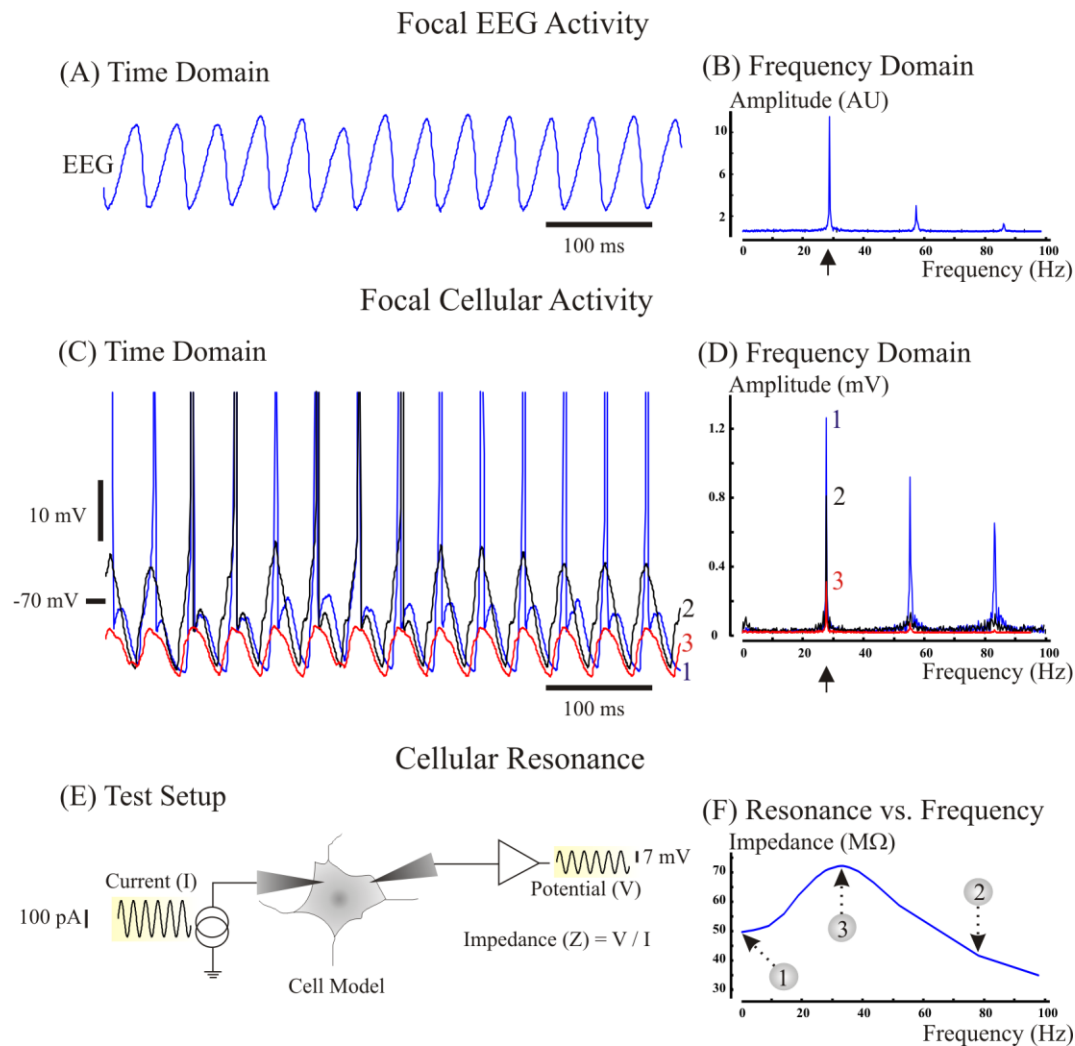


**Fig. 2:** Resonance and oscillatory activity across different levels in the model. Panels (A) and (B) show the time and frequency domain representations of the compound activity from the EEG electrode. The dominant oscillation of ~28 Hz is indicated by the arrow in panel (B). Panels (C) and (D) show oscillations in individual superficial pyramidal cells during the same EEG epoch (spikes in (C) are truncated). These cells have different levels of activity varying from non-spiking (cell 3), to occasional firing (cell 2), to continuous spiking (cell 1). The subthreshold signal component shows somewhat synchronized oscillations in all neurons, and the associated amplitude spectrum (D) shows that these oscillatory components are located at ~28 Hz (arrow), the same frequency as the EEG in panel (B). The harmonics in the amplitude

spectrum are associated with the action potentials. Single-cell resonance can be recorded by injecting currents at a range of frequencies and recording the response in the membrane potential ( $E$ ). The neuronal resonance can be expressed as the ratio of membrane potential amplitude and injected current amplitude, that is, the impedance ( $F$ ). The peak of the cellular resonance is in the same area ( $\sim 30$  Hz) as the subthreshold oscillations of the neurons and the network oscillations.

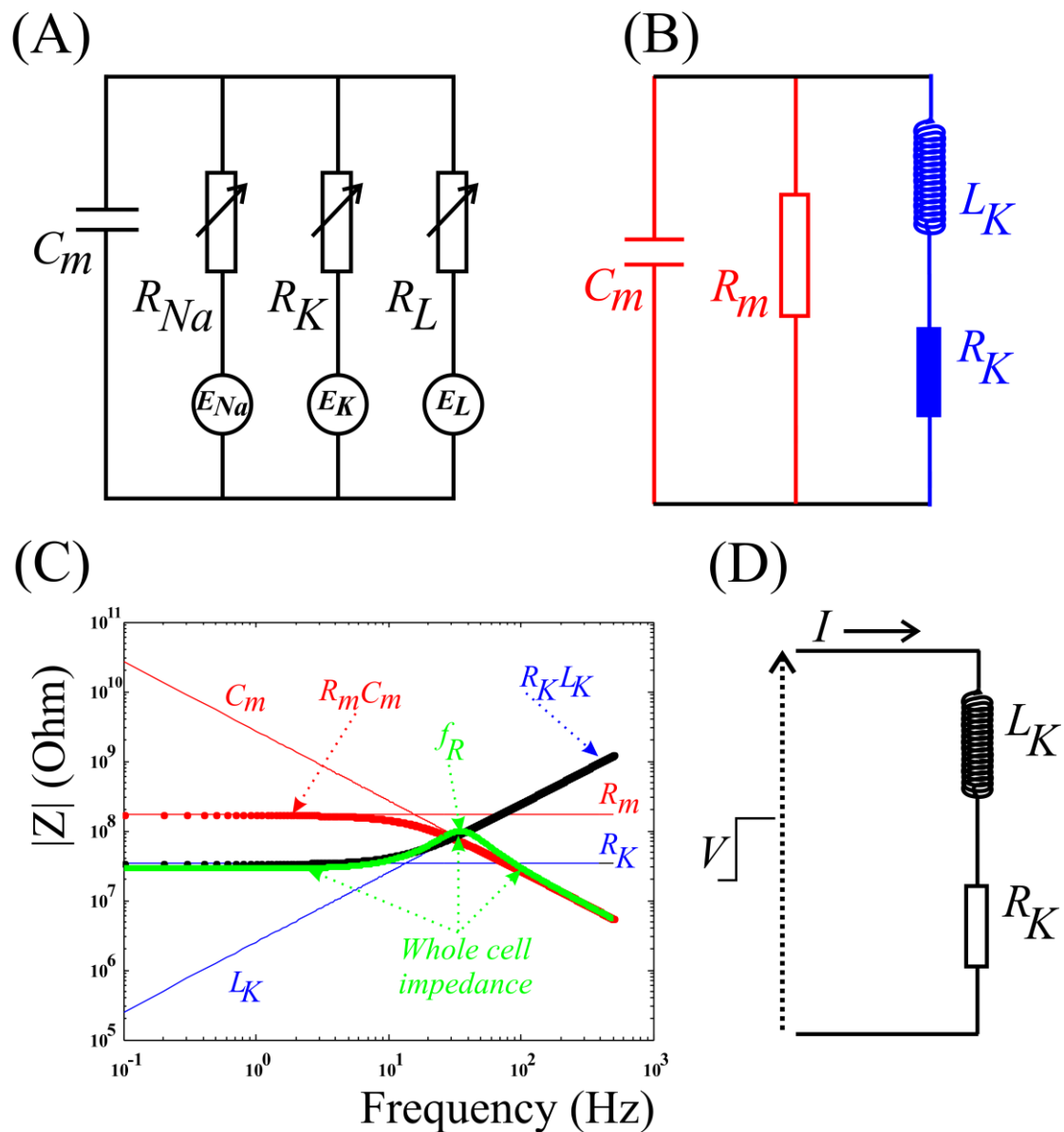


**Fig. 3:** (A) Hodgkin and Huxley neuronal membrane equivalent circuit including sodium, potassium, and leak channels (represented by  $R_{Na}$ ,  $R_K$ , and  $R_L$ , respectively).

Batteries shown represent the equilibrium potentials ( $E_{Na}$ ,  $E_K$ , and  $E_L$ ) for the respective channels. (B) Equivalent circuit model for a resonate-and-fire (RF) neuron simplified from panel (A). Batteries are omitted from the figure. (C) RF circuit elements interact to produce a peak in the impedance curve for the whole cell indicating resonance. Impedance traces are from the inductor ( $L_K$ ), resistor in series with inductor ( $R_K$ ), membrane resistance ( $R_m$ ), and membrane capacitance ( $C_m$ ). The dotted curves show the combined impedances for the  $R_m C_m$ ,  $R_K L_K$ , and the whole cell model. (D) A simplified circuit of the membrane under voltage-clamp conditions that represents the potassium channel behavior.

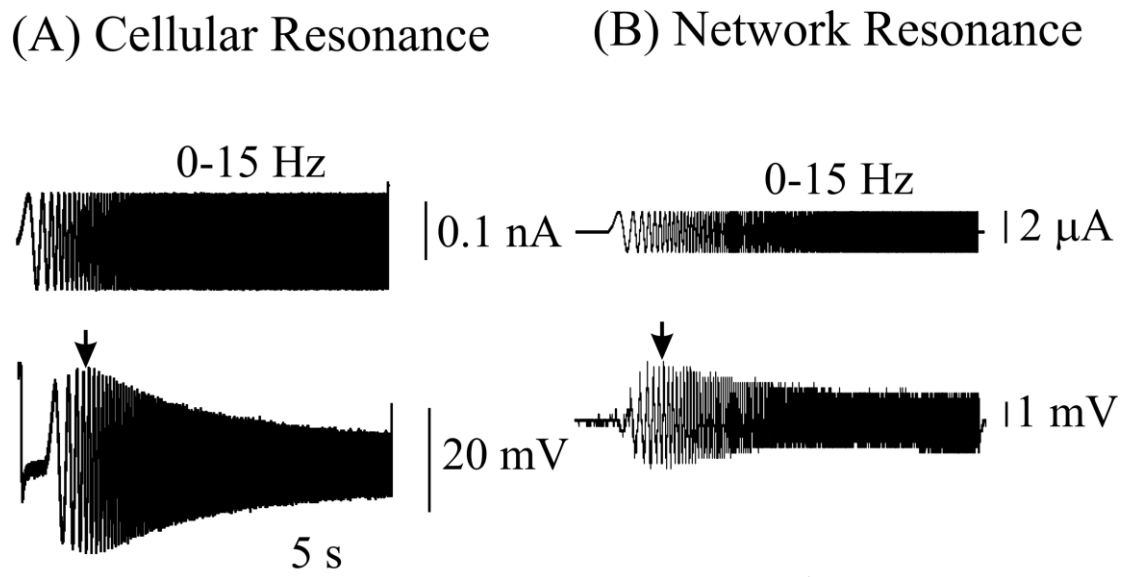


**Fig. 4:** Cellular (A) and network resonance (B) in mouse neocortical tissue in vitro. The resonance properties of real neural structures were examined by injection of a ZAP current, a signal for which the frequency increases from 0 to 15 Hz over time, top traces in panels (A) and (B). In both the cell and network we see resonance occurring at 1.6 Hz and 1.9 Hz respectively (arrows, panel (A) and (B)).

(A) Network Bursting      (B) Attenuation vs. Frequency

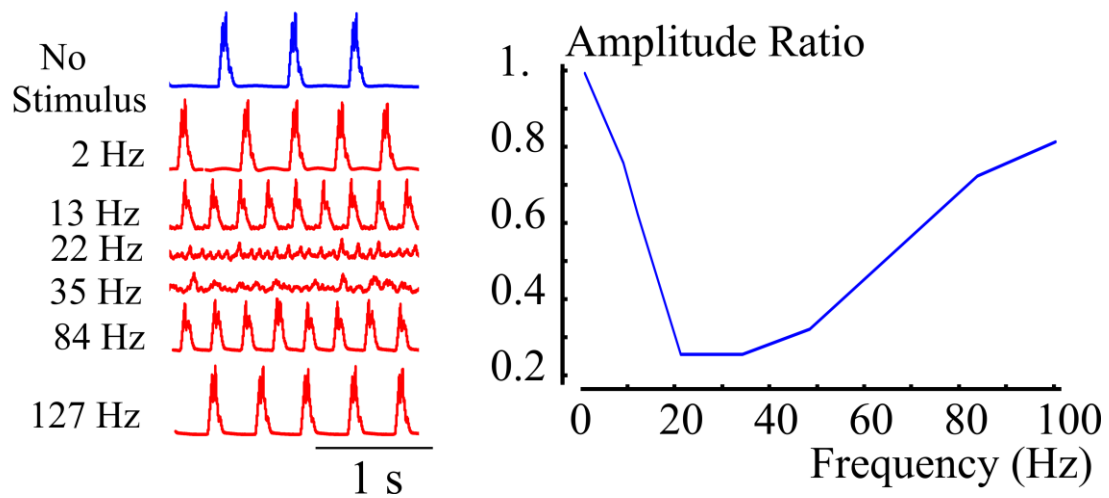


**Fig. 5:** Effect of electrical stimulation in a bursting model network. The top trace in panel (A) shows the EEG of a bursting network. When stimulating the network with sinusoidal currents at different frequencies, both the amplitude and frequency of the network bursting is affected (panel (A), six bottom traces with stimulus frequencies ranging from 2 to 127 Hz). The ratio between the amplitude of the network bursts with and without electrical stimulation is plotted versus the stimulus frequency in panel (B).

The submitted manuscript has been created by UChicago Argonne, LLC, Operator of Argonne National Laboratory ("Argonne"). Argonne, a U.S. Department of Energy Office of Science laboratory, is operated under Contract No. DE-AC02-06CH11357. The U.S. Government retains for itself, and others acting on its behalf, a paid-up nonexclusive, irrevocable worldwide license in said article to reproduce, prepare derivative works, distribute copies to the public, and perform publicly and display publicly, by or on behalf of the Government.